

Quantum motion of hydrogen on Ni(100) surfacesH. Ibach ^{*}*Peter Grünberg Institut (PGI-6), Forschungszentrum Jülich, 52425 Jülich, Germany
and Jülich Aachen Research Alliance, Aachen, Jülich, Germany*

(Received 24 August 2020; accepted 17 September 2020; published 9 October 2020)

Vibration modes of hydrogen atoms on Ni(100) are studied. The number of observed energy losses as well as their full width at half maximum (FWHM) are incompatible with the classical model of localized vibrations. Number and energy of modes agree, however, well with a previously published quantum-mechanical treatment of the motion of hydrogen in the periodic surface potential of Ni(100). For the dilute surface phase of hydrogen, the FWHM is a factor of 4 larger than expected from the dispersion of the bands. The effect is attributed to rapid tunneling of vibrationally excited hydrogen into empty neighboring sites.

DOI: [10.1103/PhysRevB.102.165405](https://doi.org/10.1103/PhysRevB.102.165405)**I. INTRODUCTION**

Dissociative hydrogen adsorption and the diffusion of hydrogen atoms on metal surfaces play a crucial role in heterogeneous catalytic processes such as synthesis of ammonia, Fischer-Tropsch synthesis of hydrocarbons, and hydrocracking. Atomic hydrogen on surfaces is of considerable technical significance also in fuel cells, in water electrolysis, and in hydrogen-induced embrittlement. Dissociation of hydrogen molecules and diffusion of hydrogen atoms on metal surfaces have therefore attracted continuous interest in the past, both in experiment and theory [1,2]. Because of the simplicity of its electronic structure, atomic hydrogen was considered a model system for adsorption [3]. However, this view point is too simple as the small mass of hydrogen gives rise to quantum effects that do not play a role for adsorbed atoms of larger mass. One example is low-temperature surface diffusion via tunneling rather than by activated hopping processes [4–7]. The relative ease of tunneling diffusion arises from the fact that the wave function of the vibration ground state of the proton partly overlaps with neighboring adsorption sites [8,9].

While the need for a quantum description is obvious for hydrogen tunneling, the vibration states of hydrogen atoms on surfaces are typically described the same way as vibrations of atoms of heavier mass, namely within the harmonic oscillator model, in which the vibrating atom is a point mass coupled to neighboring atoms. An important consequence of the local model is that vibration modes are classified according to the point group of the adsorption site. The resulting selection rules are employed for the assignment of observed spectra to specific adsorption sites [10–21]. In the case of Ni(100) surfaces, hydrogen resides in the fourfold hollow site (C_{4v} symmetry) [9,22–25]. One of the three vibration modes belongs to the A_1 representation and is therefore polarized perpendicular to the surface. The other two modes are degenerate and polarized parallel to the surface. Hence the H atom should have only two modes of different energy with the A_1 mode being the only

mode visible in infrared reflection-absorption spectroscopy or inelastic electron scattering in specular reflection (see, e.g., Sec. 7.2 of [26]).

The local model has been called into question for surfaces for which the surface potential is rather shallow. The wave function describing the position of the light hydrogen nucleus becomes rather extended in that case and a wave mechanical treatment of the motion of hydrogen atoms is required. Vibration states then become bands similar to electronic bands in the one-electron picture. A consistent wave mechanical treatment of the delocalized vibration states of hydrogen on Ni(100), Ni(111), and Ni(110) surfaces was provided by Puska *et al.* already in 1983 [9,24]. Later studies comprise hydrogen on Pt(111) [27–29], Cu(100) [8], and Rh(111) [30].

Within the band model vibrational excitations correspond to transitions between the ground state and higher energy bands. As the ground state belongs to the totally symmetric (A_1) representation all transitions between the ground state and bands of A_1 symmetry are principally visible in inelastic scattering of electrons in specular reflection. For the case of hydrogen atoms with their ground state centered in the C_{4v} site on Ni(100) Puska and Nieminen find three A_1 bands above the A_1^0 ground state and all excitations from the ground state into the three higher energy bands should have a nonzero cross section in specular-reflection inelastic electron scattering or infrared reflection-absorption spectroscopy [24]. The local model and band model therefore lead to different numbers of A_1 modes, one vs three. Whether or not quantum theory is required for the description of hydrogen motion can therefore be decided by studying the hydrogen modes at low surface coverage, for which the theory of Puska *et al.* applies. An earlier investigation of hydrogen modes on Ni(100) using electron energy-loss spectroscopy (EELS) found only one mode [13]. Hence, it seemed that the need for a quantum theory was not obvious.

Improvements in the technology of EELS [31,32] enable now spectra with orders of magnitude higher count rates, thereby improving the sensitivity for vibration modes of low cross section. It is shown in this paper that hydrogen on Ni(100) has three vibrational A_1 -type transitions in the dilute

^{*}h.ibach@fz-juelich.de

phase (neighboring C_{4v} sites primarily empty) as well as in the dense phase (neighboring C_{4v} sites primarily occupied). The number of energy losses as well as their energies are in agreement with the quantum theory of Puska *et al.* [9,24]. For the densely packed surface phase where the theory, strictly speaking, does not apply, the widths of the energy losses agree with the widths expected from the dispersion of the bands. However, for the dilute phase, the widths of the energy losses are significantly larger suggesting that an appropriate quantum theory must reach beyond the stationary solution of the protonic Schrödinger equation.

II. EXPERIMENT

The EELS spectrometer used in the present experiments is described in Refs. [31,32]. The sum of the polar angles of the beam incident on the surface $\theta^{(i)}$ and the scattered beam at $\theta^{(f)}$ is kept at 90° ,

$$\theta^{(f)} + \theta^{(i)} = 90^\circ. \quad (1)$$

Rotation of the sample by $\Delta\Theta = \theta^{(f)} - \theta^{(i)}$ changes the wave-vector transfer q_{\parallel} according to the surface wave vector conservation law,

$$q_{\parallel} = k^{(f)} \sin(\theta^{(f)}) - k^{(i)} \sin(\theta^{(i)}). \quad (2)$$

Here, $k^{(i)}$ and $k^{(f)}$ are the moduli of k vectors of the incident and scattered electron, respectively. For a reasonable compromise between a high inelastic cross section and a large range of accessible momentum transfers (requiring low and high impact energies, respectively) an electron impact energy of $E_0 = 5.5\text{eV}$ was chosen. The energy resolution was set to $\sim 6\text{ meV}$.

Ni(100) surfaces are prepared by epitaxial, pseudomorphic growth of eight-atom layer (8AL) films of fcc nickel on a Cu(100) single crystal at 300 K. The film thickness guarantees that the nickel surface is essentially as on nickel bulk material while misfit induced defects are minimal. For further details of the preparation the reader is referred to [33,34].

Hydrogen molecules dissociate upon adsorption on Ni(100) surfaces. The binding energy is about 1 eV per H_2 molecule [35]. Because of the low binding energy, a stable adsorption layer at 300 K would require high ambient pressures, too high for EELS. Hydrogen adsorption was therefore studied employing liquid-nitrogen cooling of the sample holder. The actual temperature on the crystal surface was determined via the intensity ratio of energy loss and gain signals to be $120 \pm 10\text{ K}$ [36].

III. RESULTS

We first focus on spectra obtained for exposures of 0.5 L hydrogen ($1\text{L} = 10^{-6}\text{ mbar s}$). According to Christmann this exposure should lead to a hydrogen coverage of approximately 0.1 hydrogen atom per nickel surface atom [35]. In this coverage range EELS spectra do not change with increasing or decreasing coverage other than in intensity. The spectra therefore characterize the dilute limit as considered by theory.

Figure 1. Energy-loss spectrum in specular reflection ($q_{\parallel} = 0$). The spectrum displays a single hydrogen vibration peak at 67.2 meV. The peak rides on an intense continuous back-

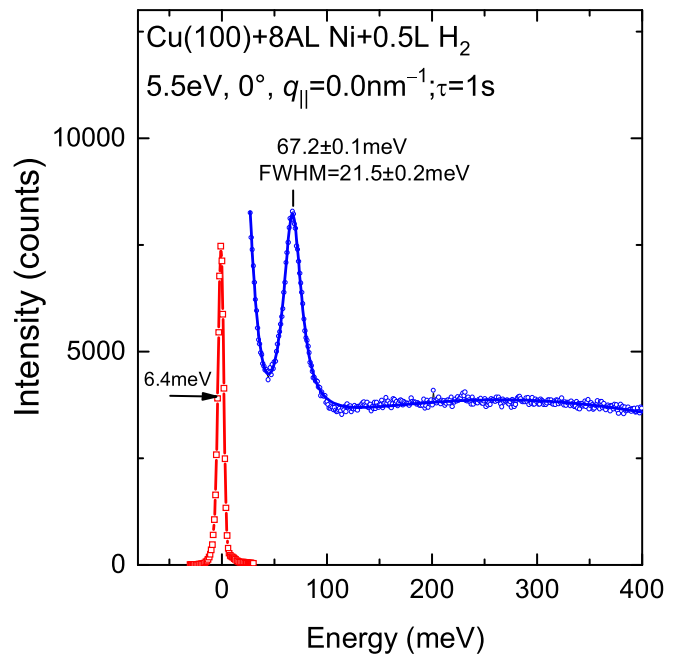


FIG. 1. Energy-loss spectrum in specular reflection at $\theta^{(i)} = \theta^{(f)} = 45^\circ$. Sampling time τ is 1s per channel. The spectrum displays a single peak at $67.2 \pm 0.1\text{ meV}$ due to atomic hydrogen. The blue solid line is a fit with a Gaussian tail for the elastic line, a Lorentzian for the hydrogen induced excitation, and a function describing the background. The fit delivers the peak count rate, the full width at half maximum (FWHM), and the energy of the hydrogen induced peak. The elastic line shown in the figure is from data for $q_{\parallel} = 7\text{ nm}^{-1}$ (Fig. 2) reduced by a factor of 15. The count rate of the in-specular elastic line is far beyond the maximum count rate accepted by the electron multiplier.

ground, which is typical for low surface conductivity metals. The background is due to dissipative electron energy losses caused by the field fluctuations induced in the surface by the probing electron [37]. The intensity of the hydrogen vibration peak and of the continuous background are focused around specular reflection (see also Fig. 3). The reason is that the electric field associated with the fluctuating dipole moments of surface excitations reaches out above the surface, and the interaction with the reflected electron takes place there. The characteristic decay length of the field scales with $1/q_{\parallel}$. The inelastic intensity due to dipole scattering is therefore concentrated on small q_{\parallel} values [26,37].

Energy losses in the off-specular direction are due to “impact scattering,” that is, they are caused by the interaction with the local potential of the hydrogen atoms (see p. 10 of [37]) and p. 351 of [26]). A sample spectrum for a wave-vector transfer of $q_{\parallel} = 7\text{ nm}^{-1}$ along the [110] ($\bar{\Gamma}\bar{X}$) direction is shown in Fig. 2. The spectrum displays three hydrogen associated losses in addition to a nickel phonon resonance around 25 meV [38].

All three hydrogen losses disappear after warming up to room temperature leaving no trace of other vibrations. This fact proves that none of the modes is due to hydrocarbon contamination since hydrocarbons would not desorb at room temperature [39]. The solid line in Fig. 2 is a fit with a

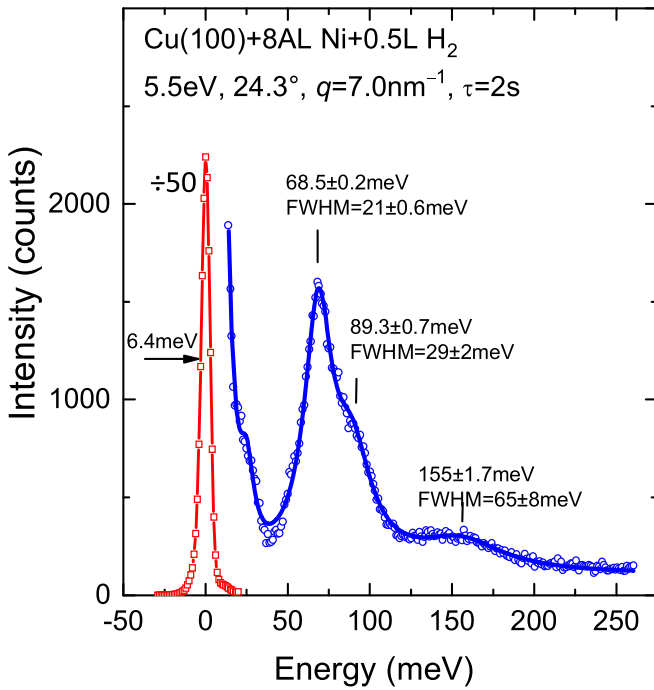


FIG. 2. Spectrum as in Fig. 1, however now for a wave vector parallel to the surface of $q_{||} = 7 \text{ nm}^{-1}$ along the [110] direction ($\theta^{(f)} - \theta^{(i)} = 24.3^\circ$). Sampling time is 2 s per channel. The elastic line is reduced by a factor of 50. The hump around 25 meV is a phonon surface resonance of Ni(100) [38].

Gaussian tail for the elastic line, a constant background, and four Lorentzians for the phonon resonance and the three hydrogen induced excitations. The fit yields the energies of the three transitions as $68.5 \pm 0.2 \text{ meV}$, $89.3 \pm 0.7 \text{ meV}$, and $155 \pm 1.7 \text{ meV}$, with the full width at half maximum (FWHM) of $21 \pm 0.6 \text{ meV}$, $29 \pm 2 \text{ meV}$, and $65 \pm 8 \text{ meV}$, respectively.

The products of peak count rates and FWHM, describing the total number of counts per second associated with a single transition (denoted as “intensity”), are plotted in Fig. 3 as function of the wave-vector transfer. The intensity of the $\sim 68\text{-meV}$ peak (denoted as A_1^1) shows the steep decrease characteristic for dipole scattering as discussed above.

For larger wave vectors $q_{||}$, in the impact scattering regime, the intensities stay roughly constant. The decline at higher wave vectors $q_{||}$ for all three peaks is presumably for a technical reason: the detection of scattered electrons emerging at a small angle with respect the surface plane is less efficient.

Figure 4 shows the peak energies as a function of the wave-vector transfer. The dispersion of the $\sim 68\text{-}$ and $\sim 89\text{-meV}$ peaks is negligible. The 158-meV excitation appears to show a downwards shift with increasing wave-vector transfer $q_{||}$. However, the full width at half maximum (FWHM) of the 158-meV energy loss (FWHM $\sim 65 \text{ meV}$) is much larger than the dispersion. In that case, the dispersion as determined by fitting depends on whether one assumes the background to be constant or decaying with energy. The dispersion for the highest energy loss as plotted in Fig. 4 may therefore be not real.

The theory of Puska *et al.* [9,24] is for a single proton in the periodic surface potential, and hence for the low coverage limit. Nevertheless, spectra for saturation coverage are like-

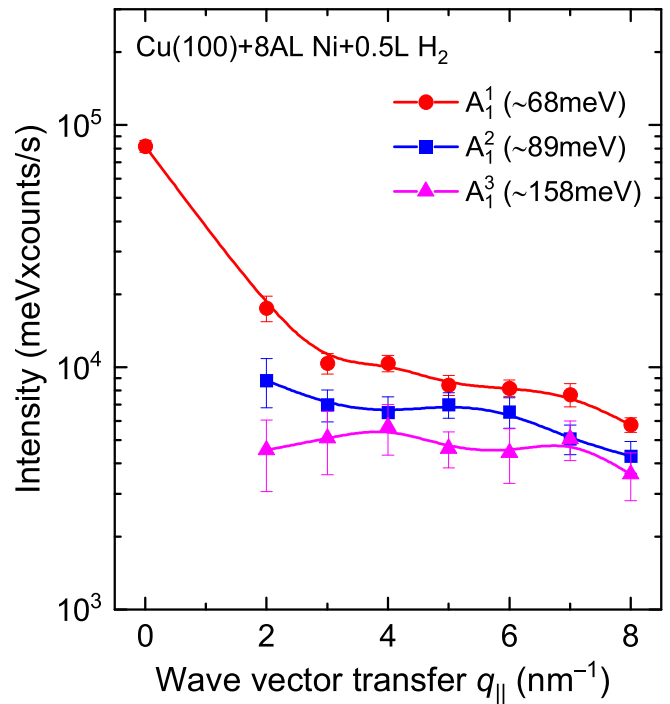


FIG. 3. Intensities of the three energy losses (peak count rate \times FWHM) as function of wave-vector transfer along the [110] ($\bar{\Gamma}\bar{X}$) direction. The steep decrease of the intensity of the 68-meV mode indicates that the cross section for inelastic scattering is dominated by electron-dipole scattering near $q_{||} = 0 \text{ nm}^{-1}$. The transitions are denoted by the final-state band (see text).

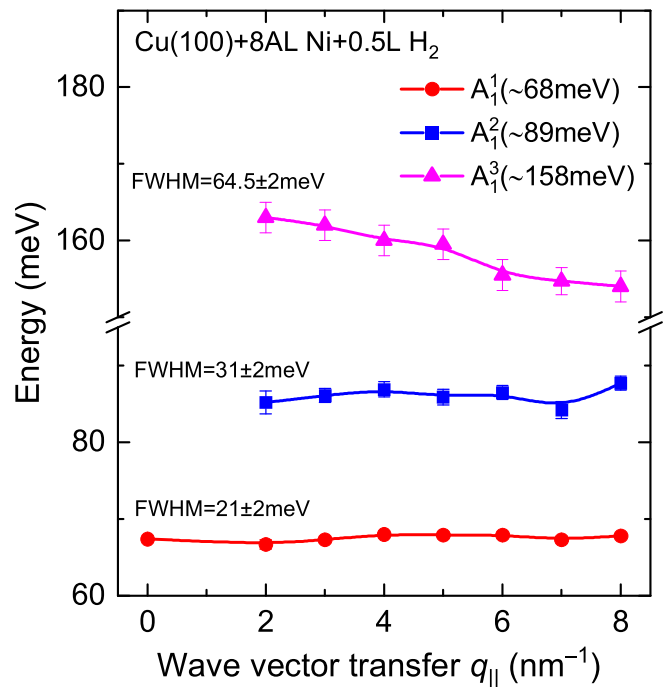


FIG. 4. Energies vs wave vector transfer for the three energy losses. Also shown is the mean full width at half maximum (FWHM) of the energy losses.

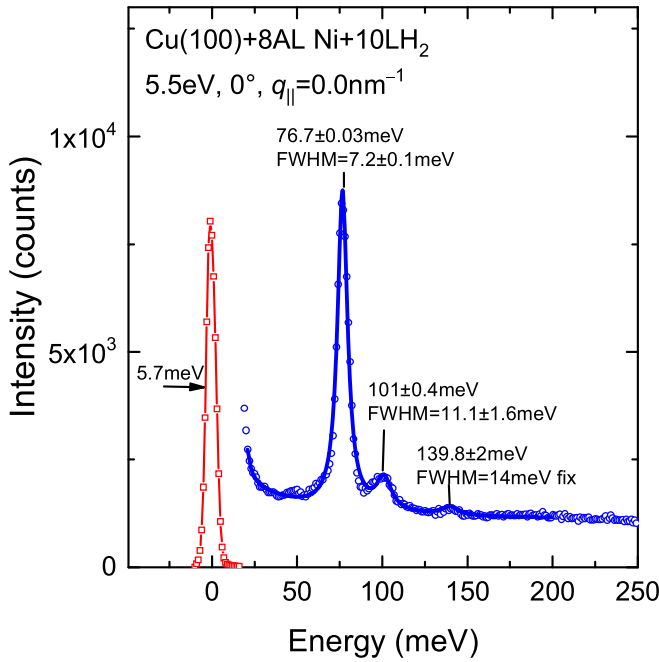


FIG. 5. Energy-loss spectrum in specular direction as in Fig. 1, however now after exposure to 10-L H_2 . Sampling time τ is 1 s per channel.

wise of interest since in that case all C_{4v} sites of the surface are occupied. That coverage is approximately obtained after exposure to 1×10^{-7} mbar H_2 for 100 s (10L) at $T \sim 120$ K [35]. Higher exposures (50 L) did not bring about further changes in the spectra. Sample spectra for $q_{\parallel} = 0 \text{ nm}^{-1}$ and $q_{\parallel} = 7 \text{ nm}^{-1}$ are shown in Figs. 5 and 6, respectively. Both

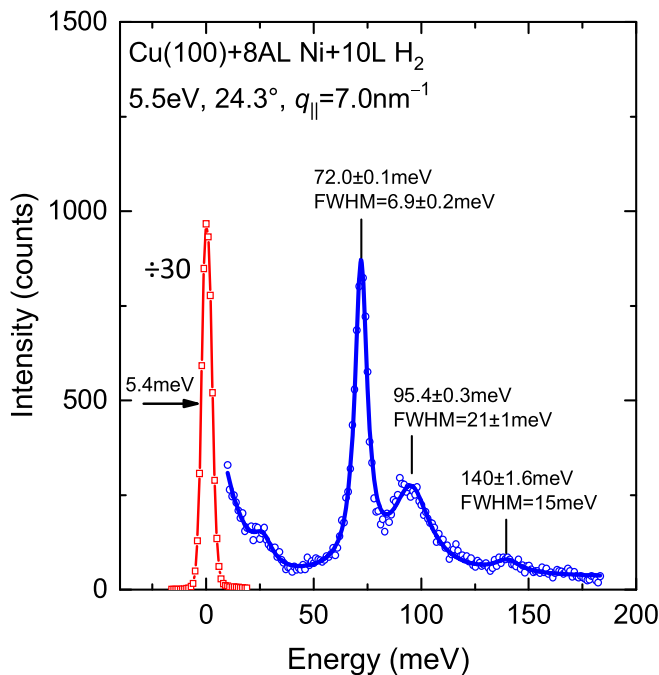


FIG. 6. Spectrum for wave-vector transfer $q_{\parallel} = 7 \text{ nm}^{-1}$ ($\theta^{(l)} = \theta^{(i)} = 24.3^\circ$) after 10 L exposure. Sampling time τ is 1 s per channel.

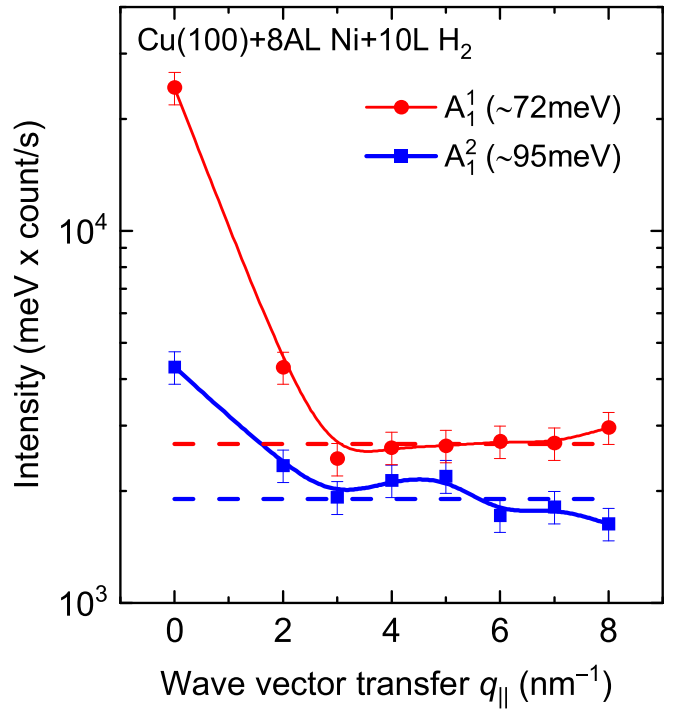


FIG. 7. Intensities of the two main energy losses as function of wave-vector transfer along the $[110]$ ($\bar{\Gamma}\bar{X}$) direction. The intensity near $q_{\parallel} = 0 \text{ nm}^{-1}$ is due to dipole scattering for both energy losses. The dashed lines are the average contribution of impact scattering.

spectra display a well separated triple of excitations, all due to atomic hydrogen. The separation of the peaks is better than in the dilute phase, primarily since the FWHMs are smaller. For example, the main peak at $q_{\parallel} = 0 \text{ nm}^{-1}$ has a FWHM of only 7.2 meV (Fig. 5). Unfolding the Lorentzian peak numerically with the Gaussian resolution function yields the true width of the excitation to be only about 5 meV, which is a factor of 4 narrower than the FWHM of the peak in the dilute phase (Fig. 1).

Comparison of Figs. 5 and 6 shows that the high-energy peak at about 140 meV shows no dispersion whereas the two lower energy peaks display a small downward dispersion. We note that the mode found here at 101 meV in the specular direction is not to be confused with the feature observed by Okuyama *et al.* in roughly the same energy range, however for much higher electron impact energies and only in the off-specular direction [40,41]. The latter mode is silent in the specular direction and disperses upward from about 85 to 106 meV at the \bar{X} point. The mode was therefore attributed to the degenerate parallel mode (excitation into an E band in the quantum picture).

Since the peaks are well resolved for saturation coverage the intensity of the second energy loss can be separated from the first even in specular reflection. Figure 7 shows the intensities (peak count rate \times FWHM) vs q_{\parallel} . The steep increase of the intensity near the specular direction demonstrates that electron-dipole scattering dominates for the A_1^1 and the A_1^2 mode near $\bar{\Gamma}$. The dipole contribution to the A_1^2 mode is about 1/9 of the dipole contribution of the A_1^1 mode. The dipolar intensity scales with the square of the dipole moment [37].

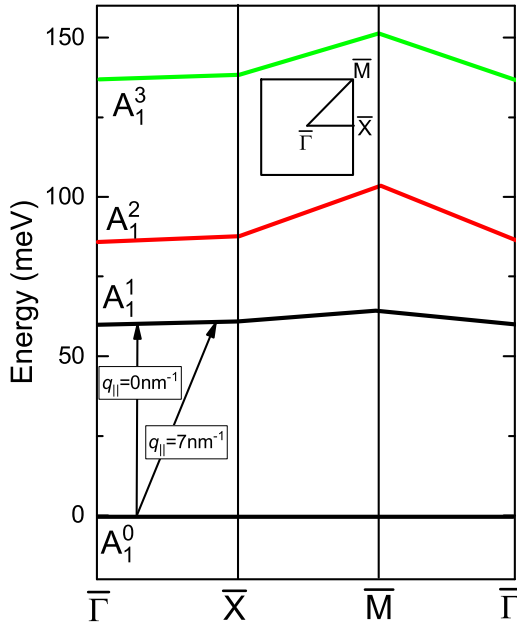


FIG. 8. Vibration band structure of a single hydrogen atom on Ni(100) (reproduced from [9]). The inset depicts the surface Brillouin zone. The ground state A_1^0 is at -2.6 eV (zero-point motion included). Examples of transitions for $q_{||} = 0 \text{ nm}^{-1}$ and $q_{||} = 7 \text{ nm}^{-1}$ are shown as arrows.

Hence, the dipole moment associated with the A_1^2 mode is one-third of the dipole moment associated with the A_1^1 mode.

Spectra for intermediate exposures are approximately a combination of the spectra of the low and high coverage phase. The concurrent presence of two phases was already observed by Karlsson *et al.* [13].

IV. ANALYSIS OF DATA

Theoretical calculations agree that on Ni(100) the fourfold hollow (C_{4v}) site has the highest binding energy for hydrogen [7,9,22–25]. Within the classical model of localized vibrations, a single atom in a C_{4v} site has only two modes of different energy, instead of three. Furthermore, only a single mode, the A_1 mode, would be active in specular reflection, regardless of the scattering mechanism (dipole scattering or impact scattering) [26,37]. The vibration spectra are therefore incompatible with the local model for the vibrations of hydrogen atoms.

The existence of three energy losses in the vibration spectra is, however, consistent with the solution of the Schrödinger equation for a single proton in the potential provided by the substrate surface atoms [9,24]. For easier reading, the band structure for hydrogen motion on Ni(100) as calculated by Puska *et al.* [9] is reproduced here in Fig. 8.

Vibration energy losses at $q_{||} = 0$ correspond to a (weighted) sum of all vertical transitions from the ground state A_1^0 into A_1^1 , A_1^2 , and A_1^3 bands. For nonzero $q_{||}$, the sum is over nonvertical transitions of the type depicted in Fig. 8. As the bands are nearly flat in the $\bar{\Gamma}\bar{X}$ direction little dispersion of the transition energies as a function of $q_{||}$ is expected, which agrees with experiment as presented here. The theoretical

TABLE I. Comparison of theory and experiment for the transition energies averaged over the $\bar{\Gamma}\bar{X}$ direction.

Transition	Theory [24]	Dilute phase	Dense phase
$A_1^0 \rightarrow A_1^1$	60 meV	67 meV	74 meV
$A_1^0 \rightarrow A_1^2$	87 meV	86 meV	96 meV
$A_1^0 \rightarrow A_1^3$	138 meV	158 meV	145 meV

transition energies in the $\bar{\Gamma}\bar{X}$ direction are listed in Table I together with the experimental values for the dilute and the dense phase averaged over the $\bar{\Gamma}\bar{X}$ direction.

The agreement between the experimental vibration energies of the dilute phase and theory is rather satisfactory. It is noted in passing that Puska *et al.* assigned the $A_1^0 \rightarrow A_1^1$ transition to the ~ 76 -meV energy loss, which was the only one experimentally observed at the time for a dense H layer [13].

According to Puska *et al.* [24] the impact scattering matrix elements for the transitions from the ground state into the A_1^1 , the A_1^2 , and the A_1^3 bands should scale as 1:0.5:0.1, respectively. This calculated sequence of intensities is roughly consistent with the sequence of intensities of the energy losses in the off-specular direction, which on the average is 1:0.7:0.25 (see Fig. 3).

For spectra in-specular reflection the change in the dipole moment perpendicular to the surface between the initial and final state of the transition is relevant. Using Fig. 5 of Ref. [24] the centroids of the vertical position of the proton are calculated as $1.81a_B$, $2.22a_B$, and $2.01a_B$, for the A_1^0 ground state, the A_1^1 state, and the A_1^2 state, respectively. Hence, there is a consi $1.81a_B$ derable shift in the mean vertical position of the proton associated with the transition, and therefore a change in dipole moment. The position shift of the proton in the $A_1^0 \rightarrow A_1^2$ transition, and hence the dipole moment associated with the transition, is about one-half of the dipole moment associated with the $A_1^0 \rightarrow A_1^1$ transition. This is in qualitative agreement with experiment.

In the absence of any other broadening mechanism the FWHM of the energy losses should be given by the width of the corresponding final-state bands (Fig. 8). That is indeed the case for the dense phase (Table II). For the dilute phase,

TABLE II. Comparison of the width of the final-state bands with the experimental FWHM for high and low coverage. For the dense phase the FWHM of the $A_1^0 \rightarrow A_1^1$ and $A_1^0 \rightarrow A_1^2$ transitions are calculated by numerical deconvolution using the Gaussian resolution function obtained from the elastic line. For the $A_1^0 \rightarrow A_1^3$ transition the signal-to-noise ratio is not high enough to extract a reliable value of the FWHM.

Transition	Theory [24]	Dilute phase	Dense phase
$A_1^0 \rightarrow A_1^1$	5 meV	21 meV	5 meV
$A_1^0 \rightarrow A_1^2$	18 meV	31 meV	20.5 meV
$A_1^0 \rightarrow A_1^3$	14 meV	64 meV	

however, the FWHMs of the energy losses are much larger, and the larger the vibration frequency, the larger the FWHM is (Table II).

In the search for a possible reason for the large FWHM in the dilute phase one might consider a strong interaction with electronic excitations [42–44]. This broadening mechanism, however, causes a Fano-type line shape for which there is no indication in the data. Another mechanism is therefore suggested here: The measured activation energy for diffusion for hydrogen on Ni(100) (across the bridge site) is only 170 meV [45]. Thus, once the hydrogen atom is in the ~ 160 -meV vibration band it tunnels rapidly into a neighboring C_{4v} site, if that site is not occupied. For the lower vibration bands the barrier of 170 meV is reduced by a lesser amount leading to less efficient tunneling. Hence, for the dilute phase, one expects a very short lifetime for the ~ 160 -meV vibration band, and longer lifetimes (smaller FWHM) for the lower energy bands, as observed. For the dense phase the neighboring C_{4v} sites are occupied; tunneling into a neighboring C_{4v} site is then blocked. The FWHMs of the energy losses of the dense phase therefore match the widths of the final-state bands (Table II). The blocking effect is akin to the well-known Coulomb blockade in electron tunnel devices (see, e.g., [46], p. 75ff).

V. CONCLUSION

Both for the dilute and the dense phase of hydrogen on Ni(100) the local model for the vibrations makes qualitative false predictions as to the number of modes to be observed. Instead, the number of observed vibrations agrees with the stationary solution of the Schrödinger equation for a single proton in the periodic potential of the surface [9]. Within that theory, the width of the vibration levels should match the width of the final-state band. That is the case for the dense hydrogen phase. However, for the dilute surface phase, for which the theory is designed, the experimental FWHM of the vibrational transitions are a factor of 4 broader than predicted by the dispersion of the bands. The broad widths are tentatively attributed to rapid tunneling of hydrogen in the vibrationally excited state into neighboring sites if these sites are not occupied. A quantitative understanding must await further theoretical investigations.

ACKNOWLEDGMENTS

Critical reading of the manuscript and valuable suggestions for improvements by M. Giesen and K. Christmann are gratefully acknowledged. The Cu(100) crystals were skillfully prepared by C. Funk.

-
- [1] K. Christmann, *Surf. Sci. Rep.* **9**, 1 (1988).
 - [2] A. Groß, *Surf. Sci.* **606**, 690 (2012).
 - [3] P. Nordlander, S. Holloway, and J. K. Nørskov, *Surf. Sci.* **136**, 59 (1984).
 - [4] S. C. Wang and R. Gomer, *J. Chem. Phys.* **83**, 4193 (1985).
 - [5] A. Auerbach, K. F. Freed, and R. Gomer, *J. Chem. Phys.* **86**, 2356 (1987).
 - [6] L. J. Lauhon and W. Ho, *Phys. Rev. Lett.* **85**, 4566 (2000).
 - [7] T. R. Mattsson, G. Wahnström, L. Bengtsson, and B. Hammer, *Phys. Rev. B* **56**, 2258 (1997).
 - [8] P. G. Sundell and G. Wahnström, *Phys. Rev. B* **70**, 081403(R) (2004).
 - [9] M. J. Puska, R. M. Nieminen, M. Manninen, B. Chakraborty, S. Holloway, and J. K. Nørskov, *Phys. Rev. Lett.* **51**, 1081 (1983).
 - [10] H. Froitzheim, H. Ibach, and S. Lehwald, *Phys. Rev. Lett.* **36**, 1549 (1976).
 - [11] R. F. Willis, W. Ho, and E. W. Plummer, *Surf. Sci.* **80**, 593 (1979).
 - [12] W. Ho, N. J. DiNardo, and E. W. Plummer, *J. Vac. Sci. Technol.* **17**, 134 (1980).
 - [13] P. A. Karlsson, A. S. Mårtensson, S. Andersson, and P. Nordlander, *Surf. Sci.* **175**, L759 (1986).
 - [14] N. J. Dinardo, G. B. Blanchet, and E. W. Plummer, *Surf. Sci.* **140**, L229 (1984).
 - [15] B. Voigtländer, S. Lehwald, and H. Ibach, *Surf. Sci.* **208**, 113 (1989).
 - [16] E. M. McCash, S. F. Parker, J. Pritchard, and M. A. Chesters, *Surf. Sci.* **215**, 363 (1989).
 - [17] M. Balden, S. Lehwald, H. Ibach, and D. L. Mills, *Phys. Rev. Lett.* **73**, 854 (1994).
 - [18] H. Yanagita, H. Fujioka, T. Aruga, N. Takagi, and M. Nishijima, *Surf. Sci.* **441**, 507 (1999).
 - [19] H. Okuyama, T. Ueda, T. Aruga, and M. Nishijima, *Phys. Rev. B* **63**, 233403 (2001).
 - [20] K. L. Kostov, W. Widdra, and D. Menzel, *Surf. Sci.* **560**, 130 (2004).
 - [21] K. Mudiyansele, Y. Yang, F. M. Hoffmann, O. J. Furlong, J. Hrbek, M. G. White, P. Liu, and D. J. Stacchiola, *J. Chem. Phys.* **139**, 044712 (2013).
 - [22] P. Ferrin, S. Kandoi, A. U. Nilekar, and M. Mavrikakis, *Surf. Sci.* **606**, 679 (2012).
 - [23] T. H. Upton and W. A. Goddard, *Phys. Rev. Lett.* **42**, 472 (1979).
 - [24] M. J. Puska and R. M. Nieminen, *Surf. Sci.* **157**, 413 (1985).
 - [25] G. Kresse and J. Hafner, *Surf. Sci.* **459**, 287 (2000).
 - [26] H. Ibach, *Physics of Surfaces and Interfaces* (Springer, Dordrecht, 2006).
 - [27] S. C. Badescu, P. Salo, T. Ala-Nissila, S. C. Ying, K. Jacobi, Y. Wang, K. Bedürftig, and G. Ertl, *Phys. Rev. Lett.* **88**, 136101 (2002).
 - [28] G. Källén and G. Wahnström, *Phys. Rev. B* **65**, 033406 (2001).
 - [29] L. Yan, Y. Yamamoto, M. Shiga, and O. Sugino, *Phys. Rev. B* **101**, 165414 (2020).
 - [30] W. Lai and D. Xie, *Surf. Sci.* **550**, 15 (2004).
 - [31] H. Ibach and J. Rajeswari, *J. Electron. Spectrosc. Relat. Phenom.* **185**, 61 (2012).
 - [32] H. Ibach, J. Rajeswari, and C. M. Schneider, *Rev. Sci. Instrum.* **82**, 123904 (2011).
 - [33] H. Ibach and C. M. Schneider, *Phys. Rev. B* **99**, 184406 (2019).
 - [34] H. Ibach and C. M. Schneider, *Phys. Rev. B* **98**, 014413 (2018).
 - [35] K. Christmann, *Z. Naturforsch. A* **34**, 22 (1979).
 - [36] H. Ibach, *Phys. Rev. Lett.* **24**, 1416 (1970).

- [37] H. Ibach and D. L. Mills, *Electron Energy Loss Spectroscopy and Surface Vibrations* (Academic, New York, 1982).
- [38] M. Rocca, S. Lehwald, H. Ibach, and T. S. Rahman, *Surf. Sci.* **171**, 632 (1986).
- [39] G. A. Somorjai and Y. Li, *Introduction to Surface Chemistry and Catalysis* (Wiley, Hoboken, 2010).
- [40] H. Okuyama, M. Z. Hossain, T. Aruga, and M. Nishijima, *Phys. Rev. B* **66**, 235411 (2002).
- [41] M. Nishijima, H. Okuyama, N. Takagi, T. Aruga, and W. Brenig, *Surf. Sci. Rep.* **57**, 113 (2005).
- [42] Y. J. Chabal, *Phys. Rev. Lett.* **55**, 845 (1985).
- [43] J. Kröger, S. Lehwald, and H. Ibach, *Phys. Rev. B* **55**, 10895 (1997).
- [44] J. Kröger, S. Lehwald, and H. Ibach, *Phys. Rev. B* **69**, 201404(R) (2004).
- [45] S. M. George, A. M. DeSantolo, and R. B. Hall, *Surf. Sci.* **159**, L425 (1985).
- [46] H. Lüth, *Quantum Physics in the Nanoworld* (Springer Cham, Heidelberg, New York, Dordrecht, London, 2015).